Computational fluid dynamics model of rhythmic motion of charged droplets between parallel electrodes

Rudolf Flittner[1] **and Michal Přibyl**[1,†]

[1]Department of Chemical Engineering, University of Chemistry and Technology, Prague, 166 28 Prague 6, Czech Republic

A mathematical model of rhythmic motion of a charged droplet between two parallel electrodes is developed in this study. The work is motivated by recent experimental findings that report oscillatory behaviour of water in oil droplets under a direct current electric field. The model considers the presence of a charged droplet placed in a dielectric medium. The droplet is immediately attracted to the electrode with the opposite polarity. When approaching the electrode, the electric charge is electrochemically reversed within the droplet, which is then repelled to the other electrode. The entire process can periodically repeat. The model is able to track a deformable liquid–liquid interface, the dynamics of the wetting process at the electrodes and the dynamics of electrochemical charge transfer between the droplet and the electrodes. The dependences of the oscillation frequency, charge acquired by the droplet and charging time on several model parameters (surface charge density on electrodes, kinetic parameter of charging, droplet–electrode contact angle, droplet size, liquid permittivity) are examined. Qualitative agreement of the model predictions with available experimental data is obtained, e.g. the oscillation frequency increases with growing electric field strength or droplet size. Our model represents the first successful attempt to predict oscillatory motion of aqueous droplets by a pseudo-three-dimensional two-phase approach. Our model also strongly supports the theory that the oscillatory motion relies on the combination of electrochemical charge injection at the electrodes and electrostatic attraction/repulsion processes.

Key words: drops, MHD and electrohydrodynamics, micro-/nano-fluid dynamics

1. Introduction

Various microfluidic applications exploit multiphase flow of different types (Gunther & Jensen 2006; Zhao 2013). One of them, called slug or segmented flow (Cahill 2014), is often generated at T or Y bifurcations of microfluidic channels (Dessimoz *et al.* 2008) or in flow-focusing devices (Li *et al.* 2013). Two-phase flows of two immiscible liquids or gas–liquid flows are usually formed; however, more complex three-phase systems such as gas–(liquid–liquid) flows have been reported (Cech,

† Email address for correspondence: pribylm@vscht.cz

Pribyl & Snita 2013; Ladosz, Rigger & von Rohr 2016). Slug flow is characterized by continuous formation of small droplets or bubbles of one phase regularly dispersed in another immiscible phase. Droplets then move along a microfluidic channel or microcapillary. Regular separation of phases provides constant residence time of all slugs in a microfluidic device (Arndt, Thoming & Baumer 2013). Moreover, both phases are intensively stirred due to internal circulation, which has been predicted theoretically (Kashid *et al.* 2005) and confirmed experimentally (Meyer, Hoffmann & Schluter 2014). Slug flow also enhances mass transport in microreactors or microseparators due to the large interfacial area (Kashid & Agar 2007; Ghaini, Kashid & Agar 2010). There are many possibilities in terms of how to arrange a chemical reaction in a slug flow. One phase can serve as the reaction phase and the other phase as a simple separator, reservoir of reactants, catalyst or product container (Jovanovic *et al.* 2010). The chemical or biological reaction can be confined to the interface itself (Cech *et al.* 2012). Microchips for cellular and toxicology studies (Cao & Köhler 2015) and particle generators (Testino *et al.* 2015) are among other applications of slug flow microdevices.

It is necessary to reliably control droplet transport in slug flow devices. Systems of precise dosing pumps sometimes coupled with different types of valves represent classical solutions of flow control (Iverson & Garimella 2008). Flow in microfluidic devices is typically coupled with the use of expensive pumps that are able to overcome high pressure drops (Jovanovic *et al.* 2011). Electrokinetic phenomena represent alternatives to pressure-driven pumping (Wang *et al.* 2009). Aqueous electrolytes can be transported in a microfluidic structure by electroosmotic convection arising from the interaction of an imposed electric field and free electric charge formed at polarized microchannel walls; see e.g. Hrdlicka *et al.* (2010) and Hrdlicka *et al.* (2013). Here we focus on a two-phase system with an aqueous droplet placed in a dielectric medium. Link *et al.* (2006) showed that an aqueous droplet can be efficiently addressed (transported to a specific place of a microfluidic chip) by a direct current (DC) electric field of proper strength and orientation in a complex microfluidic structure. An aqueous droplet is electrically charged at an electrode by electrochemical reaction in the first step. A DC electric field is then applied between two or more electrodes properly placed in a microfluidic chip. The Coulomb force attracts the droplet to the oppositely charged electrode and thus provides the addressing (i.e. controlled droplet motion to a particular place on a microfluidic chip). The same type of droplet addressing was used, for example, in Ahn *et al.* (2009) and Ahn *et al.* (2011). Recently, the Coulombic and dielectrophoretic contributions to the total electric force in different microelectrode arrangements were evaluated, which can aid in the efficient design of addressing microdevices (Ahn *et al.* 2015). Other phenomena such as electrocoalescence and droplet breakup (Bartlett, Genero & Bird 2015) can also contribute to efficient droplet addressing.

Several research groups have reported oscillatory or rhythmic motion under a DC electric field in the system formed by an aqueous droplet, dielectric fluid and a pair of electrodes (Hase, Watanabe & Yoshikawa 2006; Jung, Oh & Kang 2008; Im *et al.* 2011, 2012; Kurimura *et al.* 2013; Mhatre & Thaokar 2013; Beranek *et al.* 2014). The oscillatory behaviour is caused by periodical injections of electric charge at one and the other electrode. Initially a charged droplet is attracted to the oppositely charged electrode. When the droplet touches the electrode, the electric charge polarity in the droplet is reversed due to a fast electrochemical reaction and the droplet is repelled back to the other electrode (Im *et al.* 2012). This process is periodic and depends on the electric field strength, composition of both phases

and geometry of the system. Rhythmic motion has been observed in systems of two horizontal rod electrodes (Hase *et al.* 2006), vertical parallel plate electrodes (Jung *et al.* 2008; Jalaal, Khorshidi & Esmaeilzadeh 2010; Im *et al.* 2011, 2012) and tip electrodes (Kurimura *et al.* 2013). The first investigation of droplet rhythmic motion in microfludic chips was reported in Beranek *et al.* (2014). It was found that the frequency of the droplet oscillations depends on the electric field strength, the ionic strength inside aqueous droplets and the electrode arrangement. The effects of the dielectrophoretic force on rhythmic motion in experimental systems with a non-homogeneous electric field have also been shown (Kurimura *et al.* 2013; Mhatre & Thaokar 2013; Beranek *et al.* 2014). Recently, it was shown that the presence of white noise enhances the regularity of droplet oscillation due to the coherent resonance phenomenon (Kurimura & Ichikawa 2016). Oscillatory behaviour in a DC electric field is not limited to aqueous droplets; for example, silver-coated glass particles were placed in a dielectric fluid and exhibited rhythmic motion, thereby providing intensive fluid mixing (Cartier, Drews & Bishop 2014).

Mathematical models of droplet motion are usually based on simple force analysis (Hase *et al.* 2006; Jung *et al.* 2008; Kurimura *et al.* 2013; Mhatre & Thaokar 2013; Beranek *et al.* 2014) or force analysis derived from a detailed knowledge of the electric field around droplets (Ahn *et al.* 2015). They can be used to estimate the amount of electric charge stored in a droplet or the effective electrophoretic mobility. However, these models are not able to reveal the flow field in both phases, the pressure distribution or the character of droplet deformation during charge reversal. The growing power of computers and powerful numerical schemes allow for simulation of complex electrokinetics and electrohydrodynamics problems such as two-phase flow under an imposed electric field, electrowetting or Taylor cone phenomena (Saville 1997; Zeng & Korsmeyer 2004; Bazant 2015; Schnitzer & Yariv 2015). Lin, Skjetne & Carlson (2012) formulated a phase field mathematical model based on the Cahn–Hilliard equation to study droplet deformation and electrocoalescence. Their two-phase model considered constant dielectric constants and conductivities in the bulk of each phase. Collins *et al.* (2013) developed a two-phase model for simulation of the Taylor cone formation and jetting of charged microdroplets from cone tips. They discovered scaling rules for the microdroplet formation. The presence of free electric charge was considered only on the interface. A spatially three-dimensional (3-D) mathematical model of slug flow under an imposed electric field was reported in Wehking & Kumar (2015). The model predicted induced deformations of flowing droplets previously observed in experiments. Wallau, Schlawitschek & Arellano-Garcia (2016) developed a two-phase flow model to study merging of aqueous droplets under an imposed electric field. The model equation considers dielectrophoretic attraction of the droplets, but the effect of free electric charge is neglected. Recently, Pillai *et al.* (2016) used Berry's model (Berry, Davidson & Harvie 2013) of two-phase flow to investigate deformation and jetting in the system formed by a droplet with ion charge carriers and an outer dielectric fluid. This model allows for the evaluation of free electric charge distribution in an electric double layer (EDL) localized at the interface. This sophisticated approach is applicable to systems with the ratio of the droplet diameter to the Debye layer thickness not much exceeding a value of one.

Here, we formulate a mathematical model of an axisymmetric cylindrical cell with an oscillating and deformable droplet. The momentum balances, together with the continuity equation and the Poisson equation, are numerically solved. To track the liquid–liquid interface, the level-set method is employed. The electrochemical
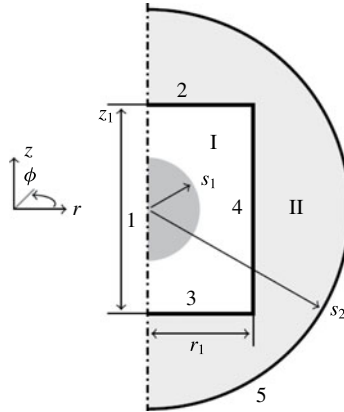
FIGURE 1. Domain geometry. Arabic and roman numerals denote boundary and domain indexes, respectively. The grey area represents the initial position of the droplet. The symbols s_1, s_2, r_1 and z_1 denote the initial droplet radius, radius of the grounded electrode, radius of the circular electrodes and spacing between the circular electrodes.

charge injection occurring at the droplet–electrode interface is also included in the model. Although several simplifications are made, the model is able to qualitatively and meaningfully predict droplet behaviour. The paper is organized as follows. A detailed description of the model domain and governing equations and the validation of the numerical method are provided in the next section. The results and discussion section introduces the dynamics of droplet behaviour and displays snapshots of selected flow patterns. Furthermore, results of several studies focused on the effects of selected model parameters on the frequency of oscillations and other characteristics are discussed.

2. Governing equations and numerical methods

2.1. *Model domain*

To avoid 3-D dynamical simulation of the model equations, an axisymmetric geometry is considered, as shown in figure 1. The cylindrical domain I contains an aqueous droplet immersed in a dielectric fluid. The domain is surrounded by circular electrodes (boundaries 2 and 3), a solid wall (boundary 4) and the axis of symmetry (boundary 1). The droplet moves between the electrodes, where it undergoes charge reversal due to electrochemical reactions. We assumed that the entire domain I is placed in a dielectric medium (domain II) surrounded by a ground electrode.

2.2. *Governing equation and the main assumptions*

Because both liquids in domain I are incompressible and Newtonian, the velocity and pressure fields are described by the Navier–Stokes and continuity equations

$$\rho \left(\frac{\partial \boldsymbol{v}}{\partial t} + \boldsymbol{v} \cdot \boldsymbol{\nabla} \boldsymbol{v} \right) = -\boldsymbol{\nabla} p + \mu \nabla^2 \boldsymbol{v} + \boldsymbol{f}_e + \boldsymbol{f}_s + \boldsymbol{f}_g, \tag{2.1}$$

$$\boldsymbol{\nabla} \cdot \boldsymbol{v} = 0, \tag{2.2}$$

where the symbols ρ, μ, t, p and $\boldsymbol{v}$ denote the liquid density, liquid dynamical viscosity, time, pressure and velocity vector, respectively. The symbols $\boldsymbol{f}_e$, $\boldsymbol{f}_s$ and $\boldsymbol{f}_g$ represent volume forces in the system.

The inertial term in the Navier–Stokes equations is considered because the values of the Reynolds number (*Re*) in experiments reported in Beranek *et al.* (2014) were typically higher than 10. In such cases, the inertial forces in the fluid bulk dominate the viscous forces. As will be shown in § 3.1, our simulations predict $Re > 100$ in some regimes.

The electric volume force f_e can be expressed as either the divergence of the Maxwell stress tensor (Saville 1997) or the Korteweg–Helmholtz force density (Grodzinsky 2011), which reads

$$f_e = \nabla \left(\frac{1}{2} \boldsymbol{E} \cdot \boldsymbol{E} \rho \frac{\partial \epsilon}{\partial \rho} \right) - \frac{1}{2} \boldsymbol{E} \cdot \boldsymbol{E} \nabla \epsilon + \omega \boldsymbol{E}, \tag{2.3}$$

where ϵ and ω are the fluid permittivity and volume density of free electric charge. The first term on the right-hand side of (2.3) is called the electrostriction force density and is typically lumped with the pressure gradient in (2.1), which leads to a modified definition of pressure (Saville 1997). Hence this term was not included in our study. The second and third terms come from the interactions between electric field and dipoles and between electric field and free charges, respectively. The dipole term is important in many electrohydrodynamics problems such as dielectrophoresis or droplet breakup. However, the mechanism of rhythmic droplet motion between two parallel electrodes is mainly driven by the interaction of injected free charge and imposed electric field (Jung *et al.* 2008; Jalaal *et al.* 2010; Im *et al.* 2011). If the droplet will not be in the proximity of an electrode, the net dielectric force will be close to zero and will not significantly contribute to the droplet forcing. For that reason, only the term containing free electric charge is considered in our simulations.

The formulation of the surface tension force in the form of divergence of the capillary pressure tensor f_s was adopted from Lafaurie *et al.* (1994):

$$f_s = \nabla \cdot [\gamma (\boldsymbol{I} - \boldsymbol{nn}) \delta], \tag{2.4}$$

where $\boldsymbol{I}$, $\boldsymbol{n}$, γ and δ are the unit tensor, normal vector to the liquid–liquid interface, interfacial tension and Dirac delta function (further defined in § 2.4), respectively.

The gravity volume force f_g is not involved in the Navier–Stokes equation due to the typically horizontal orientation of the microfluidic devices. In physical experiments with parallel plate electrodes, e.g. Im *et al.* (2011), a highly viscous organic phase is used as well as large electrodes and an organic phase with density similar to that of water. All these measures suppress the effect of the gravity force.

The liquid–liquid interface is tracked by means of the level-set method (Olsson & Kreiss 2005). Local values of the level-set function ψ are calculated from

$$\frac{\partial \psi}{\partial t} + \boldsymbol{v} \cdot \nabla \psi = R_{ls}. \tag{2.5}$$

The symbol R_{ls} represents a stabilizing term of the level-set method that is further discussed in § 2.4. The level-set function $\psi \rightarrow 0$ in the dielectric liquid and $\psi \rightarrow 1$ in the aqueous droplet. Physical properties of the liquids in domain I are then calculated using the level-set function

$$\alpha = \alpha_o (1 - \psi) + \alpha_w \psi, \quad \alpha = \rho, \mu, \epsilon. \tag{2.6}$$

In electroquasistatic systems (Grodzinsky 2011), the electric field $\boldsymbol{E}$ can be evaluated from

$$\boldsymbol{E} = -\nabla \phi, \tag{2.7}$$

where ϕ is the electric potential. The distribution of the electric potential is given by the Gauss law in the form of Poisson's equation,

$$\nabla \cdot (\epsilon \nabla \phi) = -\omega. \tag{2.8}$$

Due to the relatively high electrolytic conductivity of the aqueous phase, free electric charge will be collected in a thin EDL at the interface. The characteristic thickness of the EDL is called the Debye length and for a uni-univalent electrolyte (Hrdlicka *et al.* 2013) it is given by

$$\lambda = \sqrt{\frac{\epsilon RT}{2cF^2}}, \tag{2.9}$$

where R, T, c and F are the molar gas constant, temperature, electrolyte concentration and Faradaic constant, respectively. Depending on the concentration, the Debye length in aqueous system ranges from 1×10^{-10} to 1×10^{-7} m. It is difficult to numerically solve dynamical problems where geometrical dimensions are several orders of magnitude larger than the Debye thickness. Pillai *et al.* (2016) were able to simulate two-phase systems with the ratio of the droplet diameter to the Debye layer thickness equal to 25. The characteristic geometric dimensions of our system are $\sim 1 \times 10^{-3}$ m. Thus the ratio ranges from 1×10^4 to 1×10^7. Solution of such problems is nearly impossible even if boundaries are non-moving (Hrdlicka *et al.* 2010). Instead we consider that an aqueous droplet is homogeneously charged. The volume concentration of electric charge within the droplet is ω_w. This assumption makes it impossible to simulate jetting or Taylor cone formation. Moreover, the estimation of the dielectric force at the interface (not used in our study because the second right-hand term of (2.3) is neglected) would be imprecise due to a different distribution of the electric field within the droplet. However, it is still efficient to investigate the motion of electrically charged objects in an electric field and to study electrochemical charge injection at the electrodes. The volume density of free electric charge in domain I reads

$$\omega = \psi \omega_w. \tag{2.10}$$

Other approaches for the treatment of the electric charge distribution in the droplet can be taken into account. For example, the problem can be divided into electric and fluid parts. In the electric part, the electric potential inside the droplet can be set in an iterative manner in order to conserve the surface electric charge of a droplet not attached to an electrode. The obtained field of electric potential can be used in the next integration step to obtain the velocity, pressure and level-set variable distribution. This procedure is extremely time consuming. Moreover, artificial redistribution of the electric charge on the droplet surface will locally violate the velocity field (2.1) and thus also the position of the interface and shape of the droplet. Other problems of this approach originate from the properties of the level-set method. The level-set function is smooth in the spatial domain and the sharpness of the interface is given by the density of finite elements which is, of course, limited. Physical fields (electric potential, velocity, pressure) are represented by the same variables in both phases. The level-set function smoothly switches physical properties such as electric permittivity. So it is difficult and maybe impossible to define the electric potential at an exact coordinate of the interface in each integration step.

As domains I and II are not hydrodynamically coupled, only the distribution of the electric potential is necessary to determine in domain II by the Laplace equation

$$\nabla^2 \phi = 0. \tag{2.11}$$

In principle, it is not necessary to include domain II in the system geometry. However, it significantly helps with stability of the numerical simulations. One can imagine domain II as a cavity filled with air or other dielectric material and surrounded by a grounded Faradaic cage.

We have to consider electric charge balances to describe the electron transfer between the droplet and an electrode. Electrochemical reactions are typically limited by the electrochemical process itself or by mass transport under low or high overpotential (Bard & Faulkner 2001; Cervenka *et al.* 2012). Because the electric field in experiments with oscillating droplets is typically $\sim 10^5$ V m^{-1}, a regime limited by mass transport is more probable. We note that under low-intensity electric fields, one has to use Butler–Volmer kinetics or its modification to describe the process (Bard & Faulkner 2001). The following charge balance at the electrode–electrolyte interface can then be written

$$V_d \frac{\mathrm{d}\omega_w}{\mathrm{d}t} = - \int_A \boldsymbol{n} \cdot \kappa \boldsymbol{E} \, \mathrm{d}A, \tag{2.12}$$

where V_d is the droplet volume, κ is the electrolytic conductivity of the aqueous droplet (alternatively it can be understood as a mass transfer coefficient) and A is the droplet–electrode interfacial area. The electric field strength and electrolytic conductivity are spatially distributed in real aqueous droplets due to possible ionic depletion at the electrode surface under higher overpotential. Because EDL processes are not considered in this study, it is not meaningful to evaluate the distribution of electric conductivity within the droplet. Then a constant κ is assumed. Another simplification used here is that we replace the local value of $\boldsymbol{n} \cdot \boldsymbol{E}$ by the average electric field strength between the electrodes $\bar{E}$ in (2.12). The average strength is calculated as the difference of electric potential between the electrodes divided by the electrode–electrode distance. Equation (2.12) finally simplifies to the form

$$r = \frac{\mathrm{d}\omega_w}{\mathrm{d}t} = K \int_0^{r_1} 2\pi r \psi \, \mathrm{d}r. \tag{2.13}$$

The integral of the level-set function over the entire electrode surface represents the electrode–electrolyte interfacial area A. Equation (2.13) uses classical chemical engineering philosophy regarding how to describe a rate r of a complex mass transfer process. Typically $r = k\Delta XA$, where k is the mass transfer coefficient, ΔX is the driving force and A is the contact area. The driving force, i.e. the gradient of electric potential, is approximated as $\bar{E}$ and can be coupled with the constant k to yield the charging constant (effective mass transfer coefficient) K. The mass transfer coefficient k depends on geometrical parameters (droplet volume) and the effective electrolyte conductivity at the interface. The conductivity at the interface can significantly differ from a bulk value, because the appearance of an ion-depleted zone is highly probable under an intensive electric field (Slouka *et al.* 2007).

2.3. *Boundary conditions and initial conditions*

Axisymmetric boundary conditions were considered for all quantities at boundary 1; see figure 1. Reference zero electric potential is set at the boundary 5. Wetted wall boundary conditions (Comsol 2013*b*) with adjustable contact angle θ were applied to the boundaries 2, 3 and 4. Reference zero pressure is defined at a single point in domain I. Continuity of electric potential is considered at the boundaries 2, 3 and 4.

The other condition at these boundaries results from the application of Gauss's law (Grodzinsky 2011) and reads

$$\boldsymbol{n} \cdot (\epsilon_I \boldsymbol{E}_I - \epsilon_{II} \boldsymbol{E}_{II}) = \sigma_s, \qquad (2.14)$$

where σ_s denotes the surface concentration of electric charge and the suffixes are the domain indexes. The dielectric constant in domain II was set to one, i.e. $\epsilon_{II} = \epsilon_0$, where ϵ_0 is the vacuum permittivity. Zero surface charge is chosen at boundary 4. The boundaries 2 and 3 are considered to contain the same amount of electric charge σ with opposite polarity,

$$\sigma_s = \pm\sigma. \qquad (2.15)$$

Zero reference pressure and zero velocity were set as the initial conditions in domain I. The phase field function was set to 1 at the position of the aqueous droplet and to 0 elsewhere. The droplet initially did not touch any electrode and the volume charge density was set to an initial value $\omega_w = \omega_0$.

2.4. Numerical methods

Comsol Multiphysics 4.4 software (Comsol 2013a) and the Microfludics module extension (Comsol 2013b) based on the finite element method were used to solve the axisymmetric problem defined above. The solution was obtained in three steps. The solver internally initialized the level-set function in the first step, equation (2.5). The initial distribution of electric potential was then obtained by solving equations (2.8) and (2.11). Dynamical simulation of the full problem (equations (2.1), (2.2), (2.5), (2.8), (2.11), (2.13)) together with boundary conditions was carried out in the last step.

The Dirac function in (2.4) is approximated by (Comsol 2013b)

$$\delta = 6|\nabla\psi||\psi(1 - \psi)|. \qquad (2.16)$$

The stabilization term R_{ls} in (2.5) reads (Comsol 2013b)

$$R_{ls} = a_1 \nabla \cdot \left[a_2 \nabla\psi - \psi(1 - \psi)\frac{\nabla\psi}{|\nabla\psi|} \right], \qquad (2.17)$$

where $a_1 = 1 \text{ m s}^{-1}$ is the reinitialization parameter and a_2 is the parameter controlling the liquid–liquid interface thickness. The parameter a_2 was set to one-half of the maximum finite element size.

The multifrontal massively parallel sparse direct solver (Amestoy et al. 2001) was used for the elimination of large sparse matrixes. The relative tolerance was set to 1×10^{-3}. A solver based on backward differential formulae of first and second order with automatically adjusted time stepping was used for the time integration of the model equations (Hindmarsh et al. 2005). The relative tolerance of integration steps was set to 1×10^{-2}.

Spatial domains were discretized with triangular finite elements (figure 2). The mesh consists of approximately 1.7×10^4 elements. Most of them are localized in domain I (more than 1.4×10^4). The distribution of boundary elements is the following: the axis of symmetry (boundary 1, 130 elements), electrodes (boundaries 2 and 3, 51 and 51 elements), solid wall (boundary 4, 102 elements), grounding electrode (boundary 5, 104 elements).

The basic set of values of the dimensional model parameters is summarized in table 1. Values of selected parameters were systematically varied in parametric studies.
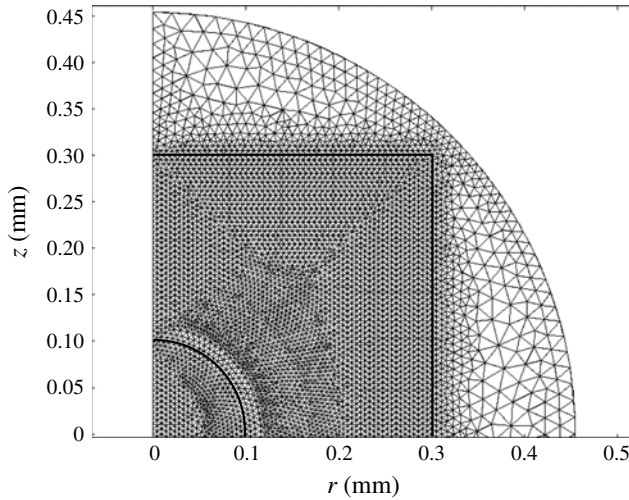
FIGURE 2. Distribution of triangular elements in one-half of the geometrical domain.

Parameter	Description	Value	Units
K	Charging constant	2.39×10^9	A m^5
r_1	Radius of circular electrodes	0.3	mm
s_1	Initial droplet radius	0.1	mm
s_2	Radius of grounded electrode	0.45	mm
z_1	Electrode–electrode spacing	0.6	mm
γ	Liquid–liquid interfacial tension	0.05	N m^{-1}
ϵ_0	Vacuum permittivity	8.854×10^{-12}	F m^{-1}
ϵ_o	Oil phase permittivity	$3\epsilon_0$	F m^{-1}
ϵ_w	Aqueous phase permittivity	$80\epsilon_0$	F m^{-1}
μ_o	Oil phase viscosity	0.001	Pa s^{-1}
μ_w	Aqueous phase viscosity	0.001	Pa s^{-1}
ρ_o	Oil phase density	800	kg m^{-3}
ρ_w	Aqueous phase density	1000	kg m^{-3}
σ	Surface charge concentration on electrodes	0.003	C m^{-2}
θ	Contact angle	130°	
ω_0	Initial volume charge density in droplet	0.5625	C m^{-3}

TABLE 1. The basic set of values of the model parameters.

2.5. *Mesh validation*

To characterize the rhythmic motion of the droplet over a longer time period, several normalized characteristics of the system were defined. The normalized volume charge density, droplet–electrode contact area and droplet position read

$$\tilde{\omega} = \omega / \max |\omega|, \tag{2.18}$$

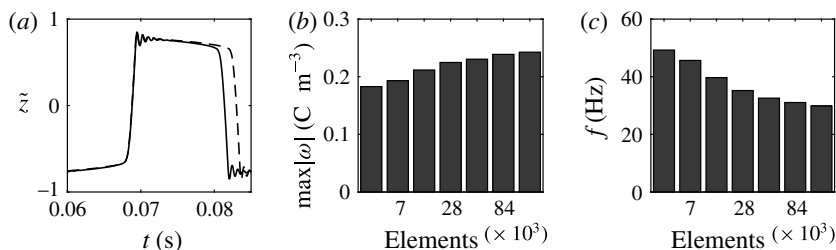$$\tilde{A} = s_1^{-2} \int_0^{r_1} 2r\psi \, \mathrm{d}r, \tag{2.19}$$

FIGURE 3. (*a*) Dependence of the normalized droplet position on time calculated with meshes consisting of 14 106 (solid line) and 28 212 (dashed line) elements in domain I. Effect of the number of mesh elements on the charge acquired by droplet (*b*) and on the frequency of droplet oscillations (*c*).

$$\tilde{z} = \frac{2 \int_{-z_1/2}^{z_1/2} \int_0^{r_1} \psi z r \, \mathrm{d}r \, \mathrm{d}z}{z_1 \int_{-z_1/2}^{z_1/2} \int_0^{r_1} \psi r \, \mathrm{d}r \, \mathrm{d}z}. \tag{2.20}$$

The volume charge density $\tilde{\omega} \in [-1, 1]$ is normalized by the maximal absolute value of volume charge density in the regular periodic regime. The contact area is normalized by the enclosed area of a circle with a radius of s_1. The droplet position is calculated as the mean integral value of the droplet position in domain I normalized by one-half of the electrode distance.

Numerical simulations of the model equations were carried out with several meshes of different quality. The corresponding normalized characteristics are plotted in figure 3. The dependences of the mean droplet position on time for the meshes with 1.4×10^4 and 2.8×10^4 elements are shown in figure 3(*a*). The dynamics of droplet transition from one electrode to the other is almost identical. The wavy parts of these time courses are also identical and correspond to damped droplet deformations that appear after touching the electrode. However, the durations of the droplet–electrode contact, i.e. the durations of electrochemical charging, differ by approximately 10 %. This results in slightly higher concentrations of free charge in the droplet (figure 3*b*) and a decreased frequency (figure 3*c*) in simulations with finer meshes. The time of droplet–electrode contact is affected by the sharpness of the liquid–liquid interface, which is always greater for a finer mesh. The droplet–electrode contact area and charge transfer are then also influenced. Because the mesh test revealed that the qualitative behaviour of the system does not depend on the mesh density and the quantitative characteristics do not differ by more than 15 % for the meshes with 1.4×10^4 and 5.6×10^4 elements, we decided to use the sparser mesh in our parametric studies. One simulation of 0.25 s time period with the mesh consisting of 1.4×10^4 elements typically took only 14 h on 4-core Intel i7-4790 3.6 GHz processors. We further repeated the simulation plotted in figure 3 for 8.4×10^4 and 1.12×10^5 finite elements. The simulation with 1.12×10^5 elements takes more than 10 days of computational time. The numerical solver uses second-order elements to approximate the velocity field and electric potential and first-order elements to approximate the pressure field (Comsol 2013*b*). The global error of numerical approximation is then directly proportional to the element size ($\sim h^1$) and convergence is rather gradual. However, the memory demands of the solver grow with
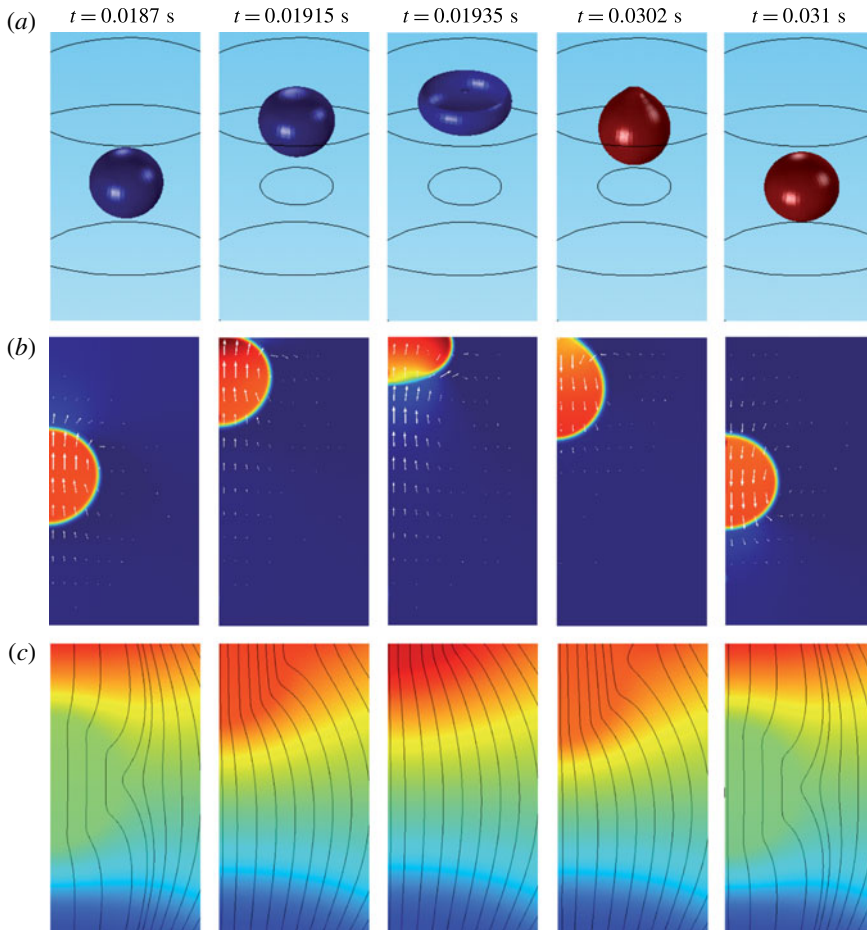
FIGURE 4. (Colour online) Snapshots of a oscillating droplet. (*a*) Droplet positions expressed as isosurface plots for $\psi = 0.5$. Droplet colour ranges from $\omega = -0.2$ C m^{-3} (blue) to $\omega = 0.2$ C m^{-3} (red). (*b*) Relative pressure distribution and velocity field. Colour palette ranges from $p = -10$ Pa (blue) to $p = 1.2$ kPa (red). White arrows indicate the vector field of velocity. (*c*) Electric field and electric potential distributions. Colour palette ranges from $\phi = -12$ kV (blue) to $\phi = 12$ kV (red). Black lines indicate the streamlines of the electric field.

$\sim h^{-2}$. The mesh consisting of 1.4×10^4 elements thus represents a good compromise between the precision of the numerical approximation and the time demands of the simulations.

3. Results and discussion

3.1. *Droplet dynamics and flow pattern*

The dynamical behaviour of a charged droplet within a dielectric fluid for the basic set of model parameters is shown in figures 4 and 5 and supplementary movie 1 available at https://doi.org/10.1017/jfm.2017.230. The movie shows the detailed dynamics of droplet deformation and interaction with solid electrodes. One can see that the charged
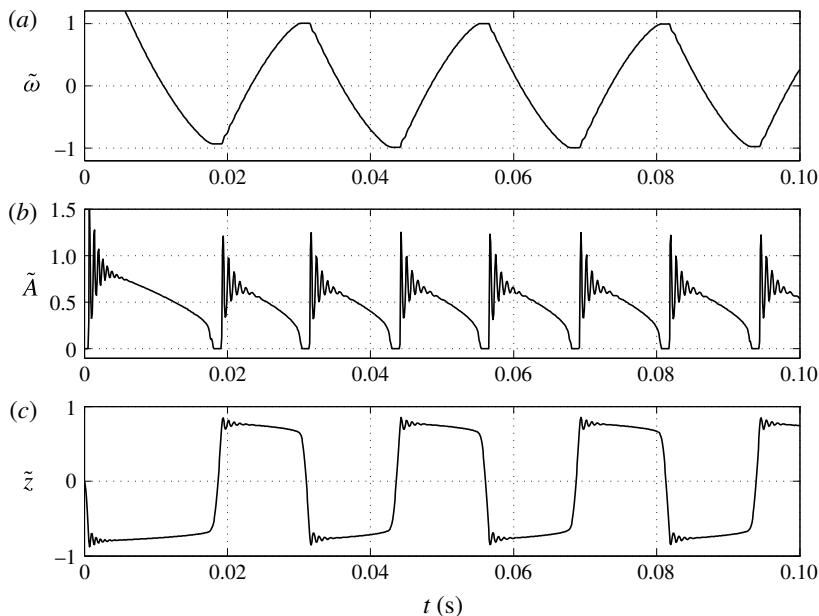
FIGURE 5. Time dependences of normalized (*a*) volume charge density, (*b*) droplet–electrode contact area and (*c*) droplet position.

droplet is attracted to the oppositely charged electrode. Once attached, the droplet–electrode interface provides a reaction area for the electrochemical reaction.

The periodic motion of droplets between electrodes consists of a charging phase, where the droplet stays at an electrode, and a non-charging phase, where the droplet moves from one electrode to the other. The charging phase can be accompanied by damped shape oscillations (movie 1) and oscillations of the droplet–electrode contact area and droplet position (figure 5). This behaviour represents a kind of damped harmonic oscillation. Damped oscillators are characterized by a linear or nonlinear damping (friction) term, which is directly proportional to the droplet or object velocity. The van der Pol oscillator represents an oscillator with a nonlinear damping term (van der Pol 1926). If forced, it can exhibit complex periodic or chaotic behaviour (Parlitz & Lauterborn 1987). The damped oscillations of droplet shape appear as a result of energy dissipation due to viscous friction in both liquids at their interface. The radial component of the velocity field is then described by spherical harmonics with a damping function $\exp(-\beta t)$, where β is the decay factor that can be estimated for different physical situations (Miller & Scriven 1968).

In relevant experiments (Hase *et al.* 2006; Jung *et al.* 2008; Im *et al.* 2011, 2012), only tiny droplet tips mediated the charge transfer across the electrode–droplet interface, which is not in full agreement with the results of our numerical simulations. However, Jalaal *et al.* (2010) observed remarkable droplet deformations in the form of damped oscillations with large contact area at the droplet–electrode interface. The droplet–electrode contact area can be reduced in our simulations, e.g. by setting higher values of the charging constant K or contact angle θ. Despite higher K or θ, the model predictions cannot be in full agreement with experimental observations, because spatially uniform droplet charging is assumed and the dielectrophoretic force neglected; see (2.12).

When the oscillations are completely damped, the interfacial area shrinks because the droplet becomes charged by electric charge of the same polarity as the electrode. At a certain moment, the electric volume force exceeds the force of interfacial tension, and the droplet is released into the dielectric fluid and moves to the other electrode. The elongation of the droplet and tip formation before the release have been observed experimentally (Jung *et al.* 2008; Im *et al.* 2011, 2012).

Damped oscillations of the droplet shape are observed after the release. Inertial forces are mostly responsible for these oscillations because the Reynolds number in this particular regime is approximately 120, which is quite far from the Stokes regime ($Re \ll 1$). Here Re is evaluated as $Re = 2\bar{v}_z s_1 \rho_w / \eta_w$, where the average axial velocity, $\bar{v}_z \approx 0.6$ m s^{-1}, is estimated as the electrode spacing z_1 divided by the duration of droplet shift between the electrodes. Similar shape deformations were observed experimentally (Beranek *et al.* 2014).

We note that a Reynolds number significantly higher than 1 is not a very common situation in microfluidics. Typical applications of droplet microfluidics such as slug flow separators or microreactors are accompanied by Stokes flow ($Re < 1$). However, in our own experiments (Beranek *et al.* 2014) Re ranged from 10 to 60, which is a result of the high frequency of oscillations; $Re = 4$ was reported in Jalaal *et al.* (2010) for a more viscous organic phase. When the inertial forces dominate over the viscous forces, the linear Stokes equation cannot be used for the description of the velocity field. However, turbulent instabilities and intermittency typically appear for $Re \sim 10^3$. Thus the description based on the nonlinear Navier–Stokes equation should be satisfactory and the solution should remain axisymmetric.

Several snapshots of domain I preceding and following the contact of a negatively charged droplet with a positively charged electrode are shown in figure 4. A nearly spherical droplet approaches the electrode. The internal pressure within the droplet is higher than that in the dielectric fluid due to the interfacial tension. The velocity field clearly indicates motion of the droplet and the surrounding dielectric liquid. The electric field is significantly deformed and the streamlines preferentially enter the droplet because of high droplet permittivity. Once the droplet touches the electrode, pressure increases due to the force reaction of the fixed electrode. The middle snapshots show the droplet in the phase of maximal deformation that is accompanied by liquid suction behind the droplet and liquid pushing next to the droplet. When the electric charge within the droplet is reversed, the droplet elongates, touching the electrode with a tiny tip. After release, the nearly spherical droplet moves back to the negatively charged electrode.

One can see that an almost regular periodic regime is attained after one charge reversal of the droplet (figure 5). The charging process is symmetric (figure 5*a*) due to the same charging constant at both electrodes. In general, the charging dynamics can be asymmetric due to different kinetics of oxidation and reduction reactions (Bard & Faulkner 2001) or asymmetric transport of ions with different electrophoretic mobilities (Grodzinsky 2011). Im *et al.* (2011) found that charging at the negative and positive electrodes differs at most by 5 %. The time dependence of the normalized contact area (figure 5*b*) is characterized by damped oscillations that emerge immediately after droplet–electrode contact as a consequence of the shape deformation. As shown in figure 5(*a*), the oscillations do not significantly affect the charging dynamics. Figure 5(*b*) further reveals that the contact area can be temporarily larger than the largest cross-sectional area of an ideally spherical droplet of the same volume. The normalized droplet position (figure 5*c*) indicates that the droplet remains in contact with the electrodes for ~ 10 ms, the duration of droplet
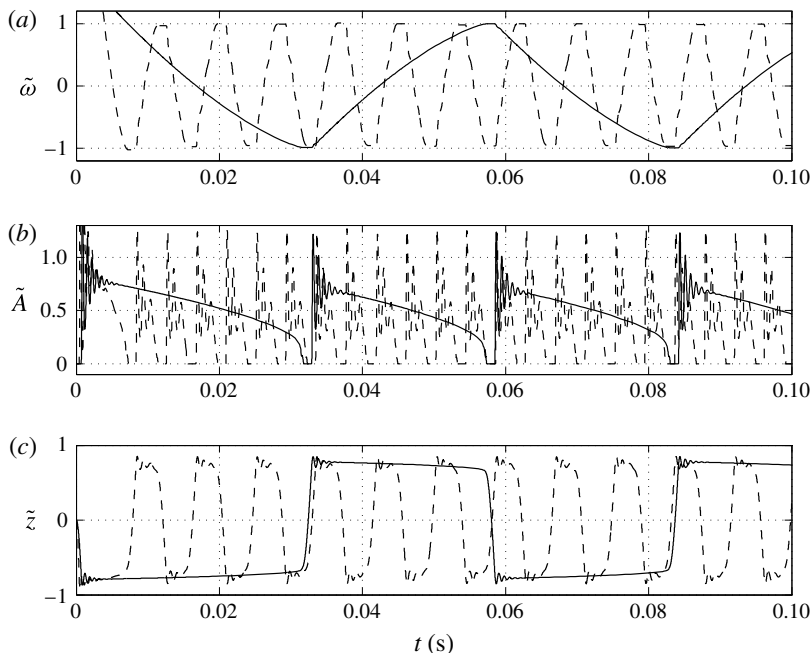
FIGURE 6. Time dependences of normalized (*a*) volume charge density, (*b*) droplet–electrode contact area and (*c*) droplet position. Solid line, $\sigma = 2$ mC m^{-2}; dashed line, $\sigma = 6$ mC m^{-2}.
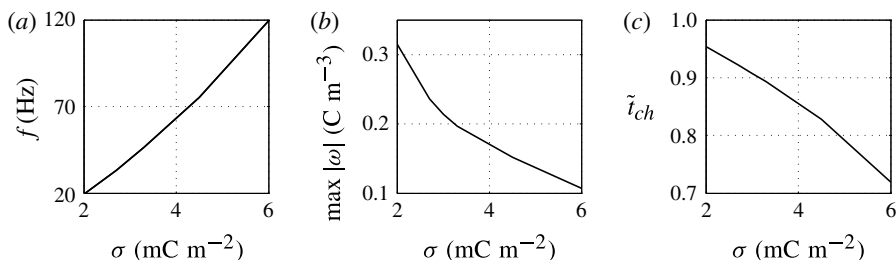

FIGURE 7. Effects of the surface charge density on (*a*) frequency of oscillations, (*b*) charge acquired by droplet and (*c*) relative time of charging.

shift between the electrodes is ~ 1 ms, and the oscillation frequency is approximately 40 Hz. The frequency of oscillations in experiments typically does not exceed 10 Hz (Hase *et al.* 2006; Im *et al.* 2012; Beranek *et al.* 2014). The difference is caused by the very high electric field strength in this particular simulation (~ 40 kV mm^{-1}). In experiments, the electric field strength is usually below 1 kV mm^{-1}. We will show in our parametric studies that the oscillation frequency decreases with decreasing electric field strength and is sensitive to other model parameters.

3.2. *Effect of surface charge density*

The higher the surface charge density on the electrodes, the higher the electric field strength forces the droplet. Monotonic increase of the oscillation frequency with the charge density is observed (figures 6 and 7). This finding is in agreement with

available experimental results (Jung *et al.* 2008; Im *et al.* 2011; Kurimura *et al.* 2013; Beranek *et al.* 2014). The dielectric effects, which are neglected in this study, are important only at the electrode surface, where instead of tiny tip formation, the droplet wets the electrode surface. This finally leads to the underestimation of the oscillation frequency because more energy is required for the droplet separation. The electric field strength affects not only the electric volume force acting on the free charge (2.1) but also the kinetics of the electrochemical reactions (2.12). This means that the droplet has to spend less time at a charging electrode to collect enough charge for detachment under a higher electric field strength; see figure 6(*c*).

In addition to frequency, two other characteristics are plotted in the parametric studies (figure 7). The charge acquired by the droplet, max $|\omega|$, is the absolute value of electric charge density acquired within one period of the stable periodic regime, and the relative time of charging, $\tilde{t}_{ch}$, is the duration of the charging process divided by the period of the stable periodic regime.

The acquired charge decreases with growing surface charge density (figure 7*b*). The electric force is the product of the electric field strength and the free charge density. Hence, a lower concentration of free electric charge is necessary to detach the droplet under a higher electric field strength. This finding is meaningful for droplets with relatively large droplet–electrode contact area. In such a case, the electric force required for droplet detachment is given by the droplet–electrode adhesion energy (expressed in the form of the contact angle σ), which is kept constant in this parametric study. However, experiments with rhythmically moving droplets forming only tiny tips during the charging showed that the acquired charge monotonically increases with the electric field strength: $\omega \propto E^{1.33}$ (Jung *et al.* 2008) or $\omega \propto E^{1.0}$ (Im *et al.* 2011, 2012). Because of negligible adhesion energy in the tip-like interaction, the electric charge concentration in a droplet grows with increasing electric field strength as the kinetics of electrochemical charging becomes faster.

The charging process is fast for high surface charge density on the electrode, which leads to a short time of charging and high frequency of droplet oscillations (figure 7*c*).

3.3. *Effect of charging parameter*

The imposed electric field affects both the electrochemical kinetics (the charging process) and the electric volume force within the charged fluid. To decouple these two phenomena, it is useful to study the influence of the charging parameter K on rhythmic motion of the droplet. The charging parameter can then be understood as an effective mass transfer coefficient multiplied by the fixed driving force ($\bar{E}$).

Figures 8 and 9 show that the larger the value of K, the higher the oscillation frequency observed. High values of the charging parameter allow for fast droplet charging, significantly reducing the time that the droplet spends at the electrode surface (figure 9*c*). Smaller values of K provide an oscillation frequency comparable to that observed in microfluidic experiments (Beranek *et al.* 2014).

In contrast with the results plotted in figure 7(*b*), the dependence of the acquired charge on the charging parameter is an increasing function (figure 9*b*). In this parametric study, the driving force $\bar{E}$ is fixed. A high value of K provides fast charge/mass transfer between the electrodes and droplet. Intensification of charge transfer is also responsible for the same trend observed in Jung *et al.* (2008) and Im *et al.* (2011, 2012).
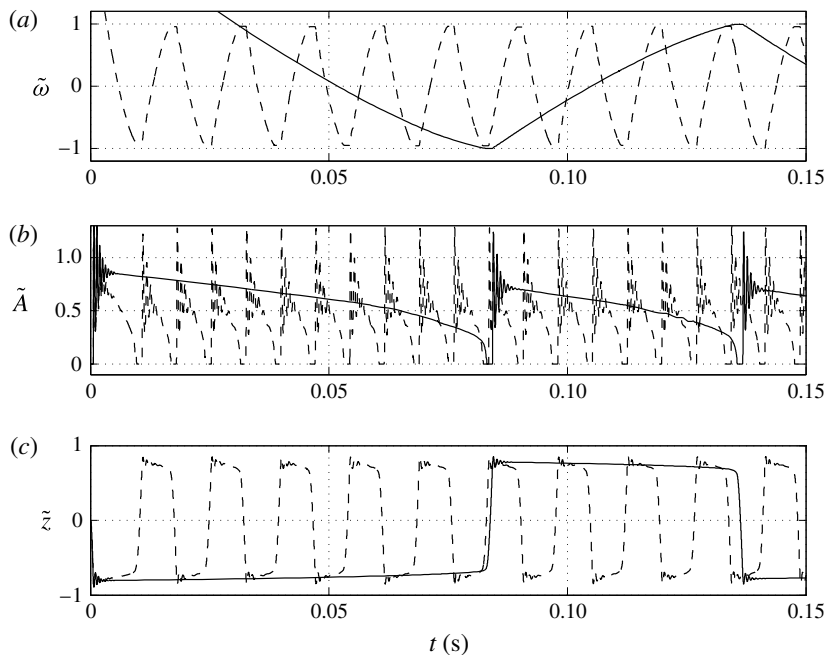
FIGURE 8. Time dependences of normalized (*a*) volume charge density, (*b*) droplet–electrode contact area and (*c*) droplet position. Solid line, $K = 0.002$ A m^5; dashed line, $K = 0.02$ A m^5.
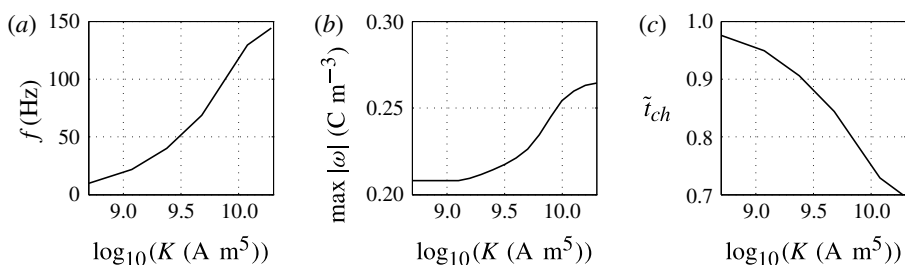

FIGURE 9. Effects of the charging parameter on (*a*) frequency of oscillations, (*b*) charge acquired by droplet and (*c*) relative time of charging.

3.4. *Effect of contact angle*

A lower value of the contact angle corresponds to a better wettability of an electrode by the droplet. While the oscillation frequency does not significantly depend on the contact angle, the electrode–droplet contact area remarkably decreases with growing contact angle; see figures 10 and 11. With larger contact area, the adhesion energy barrier increases. This has to be overcome by the electric volume force to detach the droplet. Under constant electric field strength, the force can be provided only by a larger electric charge injected into the droplet. That is the reason why the charging time is slightly longer for $\theta = 90°$ than for $\theta = 150°$ (figures 10*c* and 11*c*). The fact that the acquired electric charge monotonically decreases with the contact angle is demonstrated in figure 11(*b*).
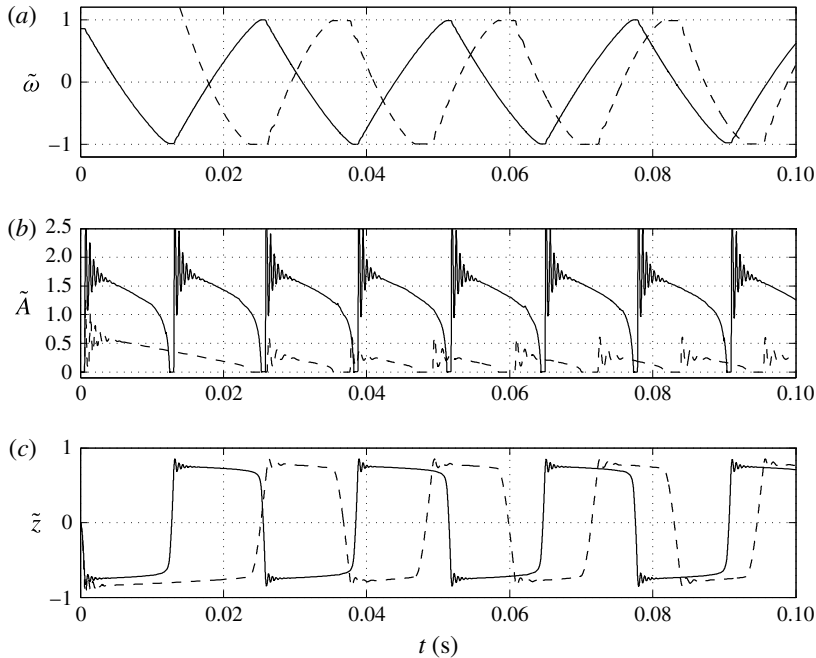
FIGURE 10. Time dependences of normalized (*a*) volume charge density, (*b*) droplet–electrode contact area and (*c*) droplet position. Solid line, $\theta = 90°$; dashed line, $\theta = 150°$.
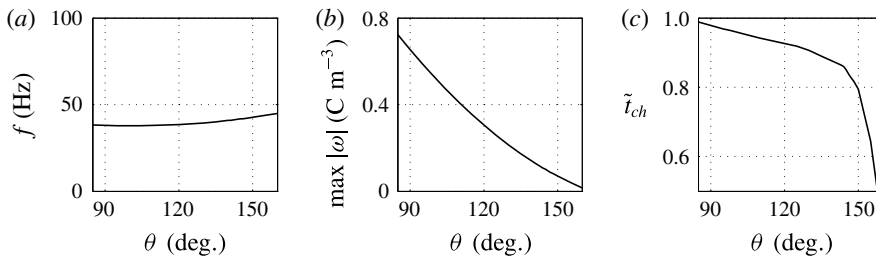

FIGURE 11. Effects of the contact angle on (*a*) frequency of oscillations, (*b*) charge acquired by droplet and (*c*) relative time of charging.

The results plotted in figures 10 and 11 are physically meaningful, however, experimental studies focused on the contact angle effects in similar experimental system have not been reported.

3.5. *Effect of droplet size*

Dependences of the velocity of oscillating droplets on the droplet radius were reported in several experimental papers (Jung *et al.* 2008; Im *et al.* 2011; Kurimura *et al.* 2013; Mhatre & Thaokar 2013). Experiments with a pair of coplanar electrodes (Jung *et al.* 2008; Im *et al.* 2011), i.e. with geometry most relevant to our theoretical study, reveal that droplet velocity and thus oscillation frequency increases with the droplet radius. Despite the fact that bigger droplets exhibit higher hydrodynamic resistances, they are able to acquire more electric charge, which increases the electric volume
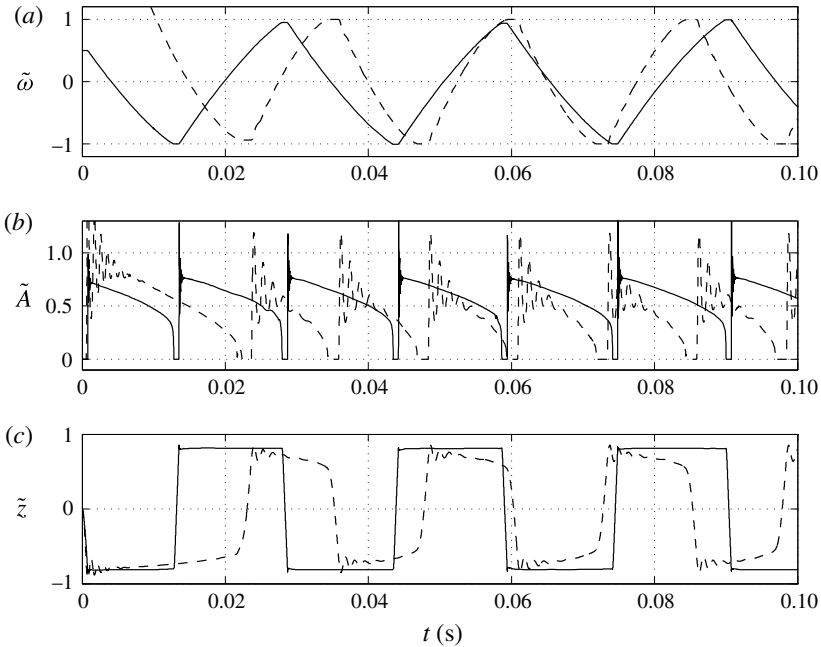
FIGURE 12. Time dependences of normalized (*a*) volume charge density, (*b*) droplet–electrode contact area and (*c*) droplet position. Solid line, $s_1 = 0.03$ mm; dashed line, $s_1 = 0.14$ mm.
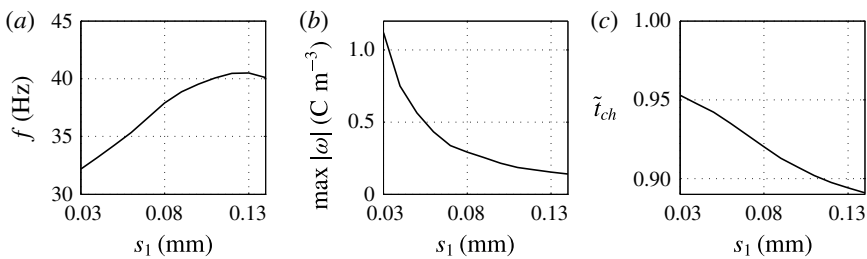

FIGURE 13. Effects of the droplet radius on (*a*) frequency of oscillations, (*b*) charge acquired by droplet and (*c*) relative time of charging.

force. These observations are in agreement with the results of numerical studies presented here; see figures 12 and 13.

Under a constant electric field, the total amount of acquired electric charge is proportional to the droplet–electrode contact area, equation (2.12), i.e. approximately $\propto s_1^2$. Droplet volume $V_d \propto s_1^3$, hence the electric charge density $\omega \propto s_1^{-1}$. This consideration is in agreement with the hyperbolic-like dependence plotted in figure 13(*b*).

As the droplet velocity is directly proportional to the total amount of acquired electric charge, the dependence of oscillation frequency on the droplet size should be approximately parabolic, $V_d \omega \propto s_1^2$. Our simulation revealed the parabolic dependence only for droplets of size less than 0.08 mm (figure 13*a*). If the droplet becomes bigger, the frequency increase is slower, then attains a maximum and finally decreases.
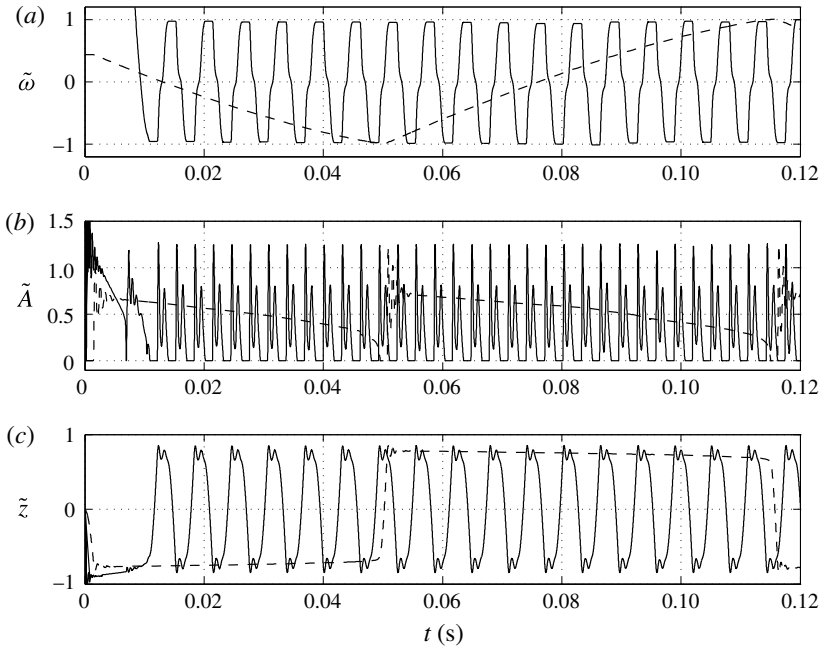
FIGURE 14. Time dependences of normalized (*a*) volume charge density, (*b*) droplet–electrode contact area and (*c*) droplet position. Solid line, $\epsilon_w/\epsilon_o = 2$; dashed line, $\epsilon_w/\epsilon_o = 210$.
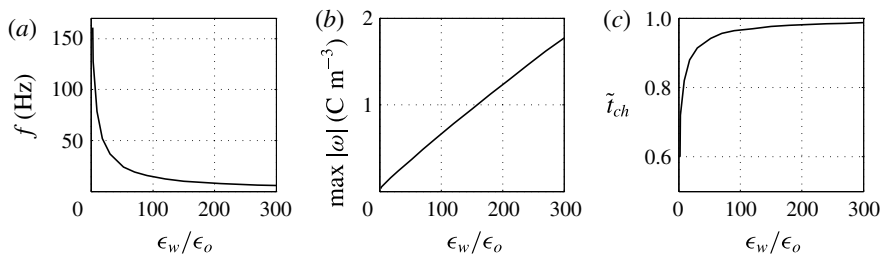

FIGURE 15. Effects of the permittivity ratio on (*a*) frequency of oscillations, (*b*) charge acquired by droplet and (*c*) relative time of charging.

This nonlinearity appears because friction forces between the droplet and the wall enveloping the two-phase system become important as $s_1 \rightarrow r_1$.

One feature of smaller droplets when touching an electrode is that there are only a few oscillations of shape. In contrast, large droplets exhibit damped oscillations during the entire period of droplet–electrode interaction (figure 12*b*), which is caused by the relatively large inertial forces.

3.6. *Effect of permittivity*

Finally, the effects of the ratio of droplet to dielectric fluid permittivities ϵ_w/ϵ_o on the character of oscillations is examined; see figures 14 and 15. The bigger the ratio, the weaker the electric field present in the charged droplet and the stronger the electric field present in the dielectric fluid. In typical experiments with water

droplets dispersed in kerosene, $\epsilon_w/\epsilon_o \approx 27$. This indicates that the electric field in the droplet is much weaker than in the dielectric fluid. This is valid not only for a homogeneously charged droplet. As a thin EDL is formed in the water phase, the electric field in the droplet bulk will be even weaker.

Figure 14 shows that high ϵ_w/ϵ_o can lead to an oscillation frequency below 10 Hz, which is typical for many reported experiments (Hase *et al.* 2006; Im *et al.* 2012; Beranek *et al.* 2014). A weaker field in the droplet results in a significant decrease of the oscillation frequency (figure 15*a*). A weaker electric field also requires more electric charge to detach the droplet from an electrode (figure 15*b*). Hence, the relative time of charging monotonically increases with ϵ_w/ϵ_o (figure 15*c*).

4. Summary and conclusion

According to our best knowledge we present a first attempt to numerically simulate a multiphysical model of a charged droplet oscillating under a DC electric field by means of computational fluid dynamics. Previously reported models relied mostly on force analysis for a rigid droplet (Hase *et al.* 2006; Jung *et al.* 2008; Kurimura *et al.* 2013; Mhatre & Thaokar 2013; Beranek *et al.* 2014). Here we show that the level-set method can be used to study the dynamics of a deformable droplet that undergoes electric charge injection at a pair of electrodes.

Despite the model simplifications, most of the obtained results are in qualitative agreement with available experimental data: (i) the charging process is symmetric on the negative and positive electrodes as observed in Im *et al.* (2011); (ii) only stable periodic regimes with period one were observed in parametric space, which is in agreement with experimental observations (Hase *et al.* 2006; Jung *et al.* 2008; Im *et al.* 2012; Kurimura *et al.* 2013; Beranek *et al.* 2014); (iii) the model predicts a monotonic increase of the oscillation frequency for growing voltage/electric field strength/surface charge density on the electrodes as reported in Jung *et al.* (2008), Im *et al.* (2011), Kurimura *et al.* (2013) and Beranek *et al.* (2014); (iv) predicted frequencies of oscillations are similar to those observed in experiments (Hase *et al.* 2006; Im *et al.* 2012; Beranek *et al.* 2014), especially for small values of the charging parameter, small densities of the electric charge on the electrodes and high ratios of permittivities of the dispersed and continuous phases; (v) the frequency of oscillations and droplet velocity increase with the droplet radius in agreement with experimental data available for coplanar electrodes (Jung *et al.* 2008; Im *et al.* 2011).

The main difference between experimental data and our theoretical predictions is found in the character of droplet–electrode interaction. The formation of only a tiny tip on the droplet surface was observed during charge injection in most of the experiments (Jung *et al.* 2008; Im *et al.* 2011, 2012; Mhatre & Thaokar 2013; Beranek *et al.* 2014). However, experiments reported in Jalaal *et al.* (2010) exhibit a large droplet–electrode interface during the charging process. Our simulations show significant wetting of electrodes by the droplet. This difference stems from two simplifying assumptions we exploited: (i) homogeneous distribution of electric charge within the droplet; (ii) the neglect of the dielectrophoretic term in (2.3). Unfortunately, to treat EDL dynamics within an aqueous droplet represents quite a difficult task due to extreme differences between the characteristic dimensions of the model domain or droplet radius on the one hand and EDL thickness or thickness of the interface on the other.

Stable periodic regimes with period one were observed in all the parametric studies reported in this paper. However, there is a possibility of the emergence of

more complex regimes in parametric space. The system is similar to dripping faucet oscillators, which frequently exhibit chaotic and higher-period regimes due to the interplay of surface tension and gravity, drag and inertial forces (Martien *et al.* 1985). Instead of the gravity force and continuous mass injection into a droplet, electric volume force and electrochemical charge injection are considered in our study.

It can be concluded that the mathematical model studied here confirms the idea that rhythmic droplet motion under a DC electric field emerges as a result of the electrochemical charging process and the interaction of free electric charge with the imposed electric field. The model is able to predict the existence of periodic oscillations in a wide region of parametric space.

Acknowledgements

Supplementary movie

A supplementary movie is available at https://doi.org/10.1017/jfm.2017.230.

REFERENCES

AHN, B., LEE, K., LOUGE, R. & OH, K. W. 2009 Concurrent droplet charging and sorting by electrostatic actuation. *Biomicrofluidics* **3** (4), 044102.

AHN, B., LEE, K., PANCHAPAKESAN, R. & OH, K. W. 2011 On-demand electrostatic droplet charging and sorting. *Biomicrofluidics* **5** (2), 024113.

AHN, M. M., IM, D. J., YOO, B. S. & KANG, I. S. 2015 Characterization of electrode alignment for optimal droplet charging and actuation in droplet-based microfluidic system. *Electrophoresis* **36** (17), 2086–2093.

AMESTOY, P. R., DUFF, I. S., KOSTER, J. & L'EXCELLENT, J.-Y. 2001 A fully asynchronous multifrontal solver using distributed dynamic scheduling. *SIAM J. Matrix Anal. Applics* **23** (1), 15–41.

ARNDT, D., THOMING, J. & BAUMER, M. 2013 Improving the quality of nanoparticle production by using a new biphasic synthesis in a slug flow microreactor. *Chem. Engng J.* **228**, 1083–1091.

BARD, A. J. & FAULKNER, L. R. 2001 *Electrochemical Methods: Fundamentals and Applications*. Wiley.

BARTLETT, C. T., GENERO, G. A. & BIRD, J. C. 2015 Coalescence and break-up of nearly inviscid conical droplets. *J. Fluid Mech.* **763**, 369–385.

BAZANT, M. Z. 2015 Electrokinetics meets electrohydrodynamics. *J. Fluid Mech.* **782**, 1–4.

BERANEK, P., FLITTNER, R., HROBAR, V., ETHGEN, P. & PRIBYL, M. 2014 Oscillatory motion of water droplets in kerosene above co-planar electrodes in microfluidic chips. *AIP Adv.* **4** (6), 067103.

BERRY, J. D., DAVIDSON, M. R. & HARVIE, D. J. E. 2013 A multiphase electrokinetic flow model for electrolytes with liquid/liquid interfaces. *J. Comput. Phys.* **251**, 209–222.

CAHILL, B. P. 2014 Introduction. In *Micro-Segmented Flow, Applications in Chemistry and Biology* (ed. M. J. Köhler & B. P. Cahill), pp. 1–6. Springer.

CAO, J. & KÖHLER, M. 2015 Droplet-based microfluidics for microtoxicological studies. *Engng Life Sci.* **15** (3), 306–317.

CARTIER, C. A., DREWS, A. M. & BISHOP, K. J. M. 2014 Microfluidic mixing of nonpolar liquids by contact charge electrophoresis. *Lab on a Chip* **14**, 4230–4236.

CECH, J., PRIBYL, M. & SNITA, D. 2013 Three-phase slug flow in microchips can provide beneficial reaction conditions for enzyme liquid–liquid reactions. *Biomicrofluidics* **7** (5), 054103.

CECH, J., SCHROTT, W., SLOUKA, Z., PRIBYL, M., BROZ, M., KUNCOVA, G. & SNITA, D. 2012 Enzyme hydrolysis of soybean oil in a slug flow microsystem. *Biochem. Engng J.* **67**, 194–202.

CERVENKA, P., HRDLICKA, J., PRIBYL, M. & SNITA, D. 2012 Kinetic mechanism for modeling of electrochemical reactions. *Phys. Rev.* E **85** (4,1), 041505.

COLLINS, R. T., SAMBATH, K., HARRIS, M. T. & BASARAN, O. A. 2013 Universal scaling laws for the disintegration of electrified drops. *Proc. Natl Acad. Sci. USA* **110** (13), 4905–4910.

COMSOL 2013a Comsol Multiphysics, Reference manual, version 4.4.

COMSOL 2013b Microfluidics module, User's guide, version 4.4.

DESSIMOZ, A. L., CAVIN, L., RENKEN, A. & KIWI-MINSKER, L. 2008 Liquid–liquid two-phase flow patterns and mass transfer characteristics in rectangular glass microreactors. *Chem. Engng Sci.* **63** (16), 4035–4044.

GHAINI, A., KASHID, M. N. & AGAR, D. W. 2010 Effective interfacial area for mass transfer in the liquid–liquid slug flow capillary microreactors. *Chem. Engng Process.* **49** (4), 358–366.

GRODZINSKY, A. J. 2011 *Fields, Forces, and Flows in Biological Systems*. Garland Science.

GUNTHER, A. & JENSEN, K. F. 2006 Multiphase microfluidics: from flow characteristics to chemical and materials synthesis. *Lab on a Chip* **6** (12), 1487–1503.

HASE, M., WATANABE, S. N. & YOSHIKAWA, K. 2006 Rhythmic motion of a droplet under a dc electric field. *Phys. Rev.* E **74** (4,2), 046301.

HINDMARSH, A. C., BROWN, P. N., GRANT, K. E., LEE, S. L., SERBAN, R., SHUMAKER, D. E. & WOODWARD, C. S. 2005 SUNDIALS: suite of nonlinear and differential/algebraic equation solvers. *ACM Trans. Math. Softw.* **31** (3), 363–396.

HRDLICKA, J., CERVENKA, P., JINDRA, T., PRIBYL, M. & SNITA, D. 2013 Mathematical modeling of traveling wave micropumps: analysis of energy transformation. *IEEE Trans. Ind. Applics* **49** (2), 685–690; Annual Meeting of the IEEE Industry Applications Society (IAS), Orlando, FL, October 09–13, 2011.

HRDLICKA, J., CERVENKA, P., PRIBYL, M. & SNITA, D. 2010 Mathematical modeling of AC electroosmosis in microfluidic and nanofluidic chips using equilibrium and non-equilibrium approaches. *J. Appl. Electrochem.* **40** (5,SI), 967–980.

IM, D. J., AHN, M. M., YOO, B. S., MOON, D., LEE, D. W. & KANG, I. S. 2012 Discrete electrostatic charge transfer by the electrophoresis of a charged droplet in a dielectric liquid. *Langmuir* **28** (32), 11656–11661.

IM, D. J., NOH, J., MOON, D. & KANG, I. S. 2011 Electrophoresis of a charged droplet in a dielectric liquid for droplet actuation. *Analyt. Chem.* **83** (13), 5168–5174.

IVERSON, B. D. & GARIMELLA, S. V. 2008 Recent advances in microscale pumping technologies: a review and evaluation. *Microfluid. Nanofluid.* **5** (2), 145–174.

JALAAL, M., KHORSHIDI, B. & ESMAEILZADEH, E. 2010 An experimental study on the motion, deformation and electrical charging of water drops falling in oil in the presence of high voltage DC electric field. *Exp. Therm. Fluid Sci.* **34** (8), 1498–1506.

JOVANOVIC, J., REBROV, E. V., NIJHUIS, T. A., HESSEL, V. & SCHOUTEN, J. C. 2010 Phase-transfer catalysis in segmented flow in a microchannel: fluidic control of selectivity and productivity. *Ind. Engng Chem. Res.* **49** (6), 2681–2687.

JOVANOVIC, J., ZHOU, W., REBROV, E. V., NIJHUIS, T. A., HESSEL, V. & SCHOUTEN, J. C. 2011 Liquid–liquid slug flow: hydrodynamics and pressure drop. *Chem. Engng Sci.* **66** (1), 42–54.

JUNG, Y. M., OH, H. C. & KANG, I. S. 2008 Electrical charging of a conducting water droplet in a dielectric fluid on the electrode surface. *J. Colloid Interface Sci.* **322** (2), 617–623.

KASHID, M. N. & AGAR, D. W. 2007 Hydrodynamics of liquid–liquid slug flow capillary microreactor: flow regimes, slug size and pressure drop. *Chem. Engng J.* **131** (13), 1–13.

KASHID, M. N., GERLACH, I., GOETZ, S., FRANZKE, J., ACKER, J. F., PLATTE, F., AGAR, D. W. & TUREK, S. 2005 Internal circulation within the liquid slugs of a liquid–liquid slug-flow capillary microreactor. *Ind. Engng Chem. Res.* **44** (14), 5003–5010; arXiv:org/10.1021/ie0490536.

KURIMURA, T. & ICHIKAWA, M. 2016 Noise-supported actuator: coherent resonance in the oscillations of a micrometer-sized object under a direct current-voltage. *Appl. Phys. Lett.* **108** (14), 144101.

KURIMURA, T., ICHIKAWA, M., TAKINOUE, M. & YOSHIKAWA, K. 2013 Back-and-forth micromotion of aqueous droplets in a dc electric field. *Phys. Rev.* E **88** (4), 042918.

LADOSZ, A., RIGGER, E. & VON ROHR, P. R. 2016 Pressure drop of three-phase liquid–liquid–gas slug flow in round microchannels. *Microfluid. Nanofluid.* **20** (3), 1–14.

LAFAURIE, B., NARDONE, C., SCARDOVELLI, R., ZALESKI, S. & ZANETTI, G. 1994 Modelling merging and fragmentation in multiphase flows with surfer. *J. Comput. Phys.* **113** (1), 134–147.

LI, Y., YAMANE, D. G., LI, S., BISWAS, S., REDDY, R. K., GOETTERT, J. S., NANDAKUMAR, K. & KUMAR, C. S. S. R. 2013 Geometric optimization of liquid–liquid slug flow in a flow-focusing millifluidic device for synthesis of nanomaterials. *Chem. Engng J.* **217**, 447–459.

LIN, YUAN, SKJETNE, PAAL & CARLSON, ANDREAS 2012 A phase field model for multiphase electro-hydrodynamic flow. *Intl J. Multiphase Flow* **45**, 1–11.

LINK, D. R., GRASLAND-MONGRAIN, E., DURI, A., SARRAZIN, F., CHENG, Z. D., CRISTOBAL, G., MARQUEZ, M. & WEITZ, D. A. 2006 Electric control of droplets in microfluidic devices. *Angew. Chem. Intl Ed. Engl.* **45** (16), 2556–2560.

MARTIEN, P., POPE, S. C., SCOTT, P. L. & SHAW, R. S. 1985 The chaotic behavior of the leaky faucet. *Phys. Lett.* A **110** (7–8), 399–404.

MEYER, C., HOFFMANN, M. & SCHLUTER, M. 2014 Micro-PIV analysis of gas–liquid Taylor flow in a vertical oriented square shaped fluidic channel. *Intl J. Multiphase Flow* **67**, 140–148.

MHATRE, S. & THAOKAR, E. M. 2013 Drop motion, deformation, and cyclic motion in a non-uniform electric field in the viscous limit. *Phys. Fluids* **25** (7), 072105.

MILLER, C. A. & SCRIVEN, L. E. 1968 Oscillations of a fluid droplet immersed in another fluid. *J. Fluid Mech.* **32** (3), 417–435.

OLSSON, E. & KREISS, G. 2005 A conservative level set method for two phase flow. *J. Comput. Phys.* **210** (1), 225–246.

PARLITZ, U. & LAUTERBORN, W. 1987 Period-doubling cascades and devil's staircases of the driven van der Pol oscillator. *Phys. Rev.* A **36** (3), 1428–1434.

PILLAI, R., BERRY, J. D., HARVIE, D. J. E. & DAVIDSON, M. R. 2016 Electrokinetics of isolated electrified drops. *Soft Matt.* **12** (14), 3310–3325.

VAN DER POL, B. 1926 LXXXVIII. On relaxation-oscillations. *Lond. Edin. Dublin Phil. Mag. J. Sci.* **2** (11), 978–992.

SAVILLE, D. A. 1997 Electrohydrodynamics: the Taylor-Melcher leaky dielectric model. *Annu. Rev. Fluid Mech.* **29** (1), 27–64.

SCHNITZER, O. & YARIV, E. 2015 The Taylor–Melcher leaky dielectric model as a macroscale electrokinetic description. *J. Fluid Mech.* **773**, 1–33.

SLOUKA, Z., PRIBYL, M., SNITA, D. & POSTLER, T. 2007 Transient behavior of an electrolytic diode. *Phys. Chem. Chem. Phys.* **9** (39), 5374–5381.

TESTINO, A., PILGER, F., LUCCHINI, M. A., QUINSAAT, J. E. Q., STAEHLI, C. & BOWEN, P. 2015 Continuous polyol synthesis of metal and metal oxide nanoparticles using a segmented flow tubular reactor (SFTR). *Molecules* **20** (6), 10566–10581.

WALLAU, W., SCHLAWITSCHEK, C. & ARELLANO-GARCIA, H. 2016 Electric field driven separation of oil-water mixtures: model development and experimental verification. *Ind. Engng Chem. Res.* **55** (16), 4585–4598.

WANG, X., CHENG, C., WANG, S. & LIU, S. 2009 Electroosmotic pumps and their applications in microfluidic systems. *Microfluid. Nanofluid.* **6** (2), 145–162.

WEHKING, J. D. & KUMAR, R. 2015 Droplet actuation in an electrified microfluidic network. *Lab on a Chip* **15**, 793–801.

ZENG, J. & KORSMEYER, T. 2004 Principles of droplet electrohydrodynamics for lab-on-a-chip. *Lab on a Chip* **4**, 265–277.

ZHAO, C. X. 2013 Multiphase flow microfluidics for the production of single or multiple emulsions for drug delivery. *Adv. Drug Deliv. Rev.* **65** (11–12), 1420–1446.